Absorption of radiation by electrons in intense magnetic fields

J. K. Daugherty and J. Ventura
I. Institut für Theoretische Physik, Universität Hamburg, 2000 Hamburg 36, Federal Republic of Germany
(Received 28 February 1977; revised manuscript received 16 May 1977)

This paper presents a quantum-mechanical treatment of photon absorption by a homogeneous electron plasma in a uniform magnetic field, in the anisotropic limit for which the electron energies are concentrated in their motion parallel to the field. The results are intended to be appropriate especially for intense fields (in which quantization effects and highly anisotropic plasmas are to be expected). The electrons are here specifically assumed to be initially in their lowest orbital states, although their parallel momenta are taken to be given by a continuous but otherwise arbitrary distribution function. It is found that the kinematical restrictions on the absorption process lead to interesting selection effects in both frequencies and polarizations, and that the photon attenuation coefficients (considered as functions of frequency and angle of incidence) can exhibit discontinuities and singularities as well as continuous features whose form and range are determined by both the field strength and the electron momentum distribution. Limiting cases of small angles and low frequencies are established, and numerical examples are postulated to illustrate these effects and suggest their significance in pulsar magnetospheres. The conditions determining the validity of the first-order approximation derived here are also investigated, and in this context the combined first-order processes of absorption and subsequent reemission are explicitly related to a corresponding resonance effect in Compton scattering.

I. INTRODUCTION

In space which is empty of external fields, energy-momentum conservation requirements forbid first-order processes (Feynman diagrams with one vertex) in quantum electrodynamics. Such processes remain forbidden in the presence of matter or other sources of microscopically varying fields, since the interactions mediated by these fields are properly described by perturbation theory as second- or higher-order effects (with single vertices describing finite momentum transfers with the external field).

In space permeated by macroscopically varying magnetic fields, however, first-order processes become possible through a continuous exchange of kinetic momentum between electrons and the external field, which is implicit in the modified wave functions governing the electron motion. The diagrams corresponding to two such effects are shown in Figs. 1(a), 1(b). The first is just the well-known process of magnetic bremsstrahlung or synchrotron radiation,[1] which is observable at least in the classical limit even for very weak fields ($\sim 10^{-5}$ G in interstellar space, for example). This is in contrast to diagram (b), which represents the field-induced conversion of a single photon into an electron-positron pair[2-4]. Intrinsically a quantum-mechanical effect, the latter process requires extremely high field strengths and photon energies well above the threshold value $\hbar\omega_{th} = 2mc^2$ to be observable (and in fact has not yet been detected in laboratory experiments).

However, since the discovery of pulsars and their subsequent interpretation as rotating neutron stars with enormously high surface magnetic fields (10^{12}–10^{13} G are often-quoted values in current pulsar models), it has been recognized that both magnetic bremsstrahlung[5,6] and magnetic pair production[7,8] may be extremely important processes in the near zones of pulsar magnetospheres. In fact, these effects may conspire together to generate electromagnetic cascade showers[7,8] on a scale large enough to influence the over-all dynamics of the magnetosphere and play a role in the mechanisms responsible for the radiation observed from these objects. More recently it has also been recognized[9,10] that the low-energy limit of magnetic bremsstrahlung (cyclotron radiation) may contribute to the radiation from pulsating x-ray sources, which are widely believed to be matter-accreting

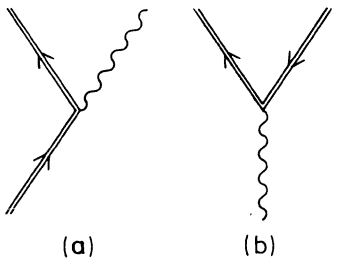

FIG. 1. First-order processes involving a single particle (electron or photon) in the initial state. The double line for the electron current denotes that the particle moves through a uniform magnetic field, so that its wave function satisfies the corresponding bound-state Dirac equation. Diagram (a) represents magnetic bremsstrahlung or synchrotron radiation, for which the emitting particle may be either a positive or negative electron. Diagram (b) denotes magnetic pair conversion of a single photon.

magnetic neutron stars in binary systems. The very recent observation by Trümper *et al.*[11] of a 53-keV line feature in the pulsed spectrum of Her X-1 may be a striking example of this emission mechanism occurring in a strongly quantizing magnetic field.[12]

Thus, the astrophysical significance of these two processes, which are also the only first-order diagrams involving a single particle (electron or photon) in the initial state, is already apparent. The object of the present work is to point out the significance of the first-order process for which both an electron and a photon are present in the initial state, and whereby the photon is absorbed to produce an electron with a higher transverse energy [as depicted in Fig. 2(a)]. It will be shown that this absorption effect may well have a critical role in the transport of radiation through the highly magnetized plasma of a neutron-star (or white dwarf) magnetosphere.

In contrast to the pair of second-order diagrams [Figs. 2(b), 2(c)] which involve the same initial states (and which represent just the Compton scattering mechanism), the first-order absorption process is characterized by highly restrictive kinematical requirements. In fact, because of the quantized nature of the electron energy states in a strong magnetic field, it is in general impossible for an electron of specified energy to absorb a photon of given frequency ω. However, for that frequency which supplies just the transition energy between two electron states (and conserves the total momentum parallel to the field direction), first-order absorption is allowed and results in a very sharp resonance in the Compton scattering cross section (due to the fact that the intermediate state in Fig. 2(b) then attains a relatively very long lifetime as a "real" particle).

At the same time it can be somewhat misleading to regard the absorption process as a resonance effect, especially in the context of a plot of the corresponding photon attenuation coefficients as functions of frequency. One of the essential points to be demonstrated in the following is that for a quasicontinuous distribution of electron momenta along the field axis, this "resonance" effect can result in first-order attenuation coefficients which appear as smeared-out functions of frequencies and angles of incidence.[13]

The goal of the present work is simply to point out the basic physical characteristics of the absorption process, and thus no attempt will be made here to deal with the full problem of radiative transport through the magnetospheric plasmas surrounding neutron stars. Instead, a more restrictive viewpoint will be adopted, in that the distribution function of a magnetized electron plasma will

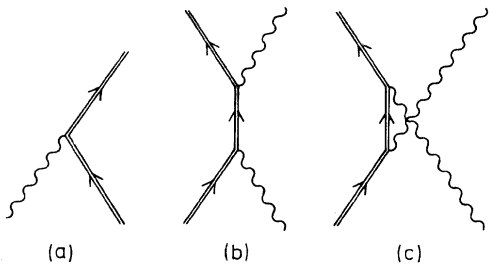

FIG. 2. (a) First-order absorption diagram. (b), (c) Compton scattering diagrams. When the kinematical conditions (6) and (7) in the text are satisfied, diagram (b) becomes equivalent to the sequential pair of diagrams 2(a) and 1(a), for which the virtual state approaches the mass shell of a real electron. Diagram (b) is responsible for the absorption resonance shown in Fig. 8 (see also Sec. VI).

be specified at the outset, and a single "test" photon will be assumed to propagate through the plasma at some angle θ with respect to the magnetic field. For present purposes, the plasma may in fact be treated simply as a gas which is homogeneous on a scale comparable with the actual spatial dimensions of the pulse of radiation here idealized as a plane-wave photon.

Two additional simplifications will be made in this initial treatment. First, plasma dispersion effects will be ignored in describing the photon wave field, so that $k_\mu k^\mu = 0$ and $a^\mu(x)$ has the form of the vacuum radiation field. This assumption limits the validity of the following results to frequencies well above the plasma frequency $\omega_p = (4\pi e^2 n_0/m)^{1/2}$, but clearly reduces the formalism to a minimum at a stage where it still remains to point out the gross features of this process. (At the same time, it should be noted that the proper inclusion of dispersive effects may not be at all straightforward: In applications dealing with the transfer of radiation between localized bunches of electrons or propagation through large-scale inhomogeneities in magnetospheric plasmas, the normal-mode fields for homogeneous plasmas would be equally inappropriate. The description of polarization effects is of course subject to the same difficulty, so that either linear or circular modes may be preferable approximations according to the specific application.) Secondly, the magnetic field strength is assumed to be sufficiently intense that it is justifiable to regard all the electrons as occupying only the lowest Landau energy levels E_0, where in general

$$E_j = (c^2p^2 + m^2c^4 + 2j\epsilon^2)^{1/2}, \quad \epsilon^2 = \frac{B}{B_{cr}} m^2c^4, \quad j = 0, 1, 2, \ldots . \tag{1}$$

However, the distribution of momenta p parallel to the field direction is not restricted, and will here be described by a distribution function $\eta(p)$ whose form is arbitrary. Thus by appropriate choices for $\eta(p)$, the results presented below may be immediately applied either to pulsar models (for which highly relativistic momenta may be of interest) or to the accretion funnels of pulsating x-ray sources (where mildly relativistic, downward-moving electrons are to be expected).

The following sections will present a derivation of the photon attenuation coefficient $\kappa(\omega, \theta)$ (inverse of the mean free path λ) against first-order absorption in the electron plasma described above. In Sec. V the results will be applied to several different forms of the possible electron spectra, which should serve to demonstrate essential features of the absorption mechanism. Section VI compares the first-order absorption with the Compton effect, and finally in Sec. VII some possible applications to realistic models of pulsars and pulsating x-ray sources are discussed.

II. FIRST-ORDER CALCULATION OF THE ATTENUATION COEFFICIENTS

Since the principal physical application of the following results is intended for pulsar magnetic fields which vary in space only over distances comparable to a neutron-star radius (~10^6 cm), it is a very good approximation to assume a uniform magnetic field $\vec{B} = B\hat{z}$. It is further assumed that the electron gas is itself uniformly distributed over both the x-y plane and along the z direction. It may be noted that no assumptions are required about the ratio of the interparticle spacings parallel and transverse to the field lines. For the calculation presented here, the particles are taken to be negatively charged electrons, but of course absorption by positrons satisfying the same distribution function would give identical results (except for reversal of the photon polarizations).

The requirement that all the electrons be in their lowest transverse energy states implies that their orbital quantum number $n = 0$ and spin quantum number $s = -1$, so that the integer $j = 2n + s + 1$ appearing in Eq. (1) for the particle energy vanishes.[14] The longitudinal momenta p are left arbitrary, and may assume both positive and negative values.

Thus the distribution function of the electron gas may be written in the form

$$f_0(p, \vec{x}, t) = n_0 \eta(p) , \tag{2}$$

where n_0 is the total number of electrons per unit volume and the one-dimensional distribution $\eta(p)$ is normalized to unity:

$$\int_{-\infty}^{\infty} dp \eta(p) = 1 .$$

The subscript 0 labeling f and n serves as a reminder that $j = 0$ for all particles.

The next step is to introduce a photon of energy ω into the gas, whose wave vector $\vec{k}$ is inclined at an angle θ to the magnetic field. (Here $\hbar = c = 1$ throughout, and in general the notational conventions used in Bjorken and Drell[15] will be adopted.) Without loss of generality, it is convenient to choose the coordinate system so that $\vec{k} \cdot \vec{x} = k(y \sin\theta + z \cos\theta)$. The photon attenuation coefficient will be calculated for the two cases of linear polarization defined by the unit vectors

$$\hat{\epsilon}_{(1)} = -\cos\theta \hat{y} + \sin\theta \hat{z} , \tag{3a}$$

$$\hat{\epsilon}_{(2)} = +\hat{x} \tag{3b}$$

(so that $\hat{\epsilon}_{(1)}$, $\hat{\epsilon}_{(2)}$, and $\hat{k}$ form a right-handed triad), as well as for the two circular-polarization vectors,

$$\hat{\epsilon}_{(\pm)} = \mp \frac{1}{\sqrt{2}} (\hat{\epsilon}_{(1)} \pm i\hat{\epsilon}_{(2)}) . \tag{3c}$$

In the perturbation calculation used here, the "photon" is regarded as a weak classical radiation field described by the potential

$$a^{\mu}(x) = \frac{\epsilon^{\mu}}{(2\omega L^3)^{1/2}} e^{-ik_{\nu}x^{\nu}} , \tag{4}$$

where $\epsilon^{\mu} = (0, \hat{\epsilon})$ and it is assumed that $\int d^4x = L^3 T$. This radiation field is superimposed on the uniform magnetic field, whose potential may be taken as

$$\bar{A}^{\mu}(x) = (0, \tfrac{1}{2}\vec{B} \times \vec{r}) . \tag{5}$$

Corresponding to the diagram in Fig. 2(a), the radiation field may scatter an electron of initial energy $E_0 = (p^2 + m^2)^{1/2}$, causing it to undergo a transition into a state $E_j = (q^2 + m^2 + 2j\epsilon^2)^{1/2}$ with $j > 0$. Since this scattering corresponds to the absorption of the photon of energy ω, the kinematical requirements to be imposed are

$$q = p + \omega \cos\theta , \tag{6}$$

$$E_j = E_0 + \omega . \tag{7}$$

These conditions will be examined more closely in Sec. III below, although their formal role in the calculation of the attenuation coefficients will soon become apparent in the present discussion.

To describe the electron in its initial and final states, wave functions discussed in detail by Johnson and Lippmann[14] will be used. Thus

$$\psi_{\text{initial}}(x) = \left(\frac{m}{E_0}\right)^{1/2} u_0(p, a; \vec{x}) e^{-iE_0 t} , \tag{8}$$

$$\psi_{\text{final}}(x) = \left(\frac{m}{E_j}\right)^{1/2} u_j^{(s)}(q, b; \vec{x}) e^{-iE_j t}, \quad s = \pm 1, \tag{9}$$

where

$$u_0 = \left(\frac{E_0+m}{2m}\right)^{1/2} \begin{bmatrix} 0 \\ \chi_0(p, a; \vec{x}) \\ 0 \\ \frac{-p}{E_0+m}\chi_0(p, a; \vec{x}) \end{bmatrix}, \tag{10a}$$

$$u_j^{(1)} = \left(\frac{E_j+m}{2m}\right)^{1/2} \begin{bmatrix} \chi_{j-1}(q, b; \vec{x}) \\ 0 \\ \frac{q}{E_j+m}\chi_{j-1}(q, b; \vec{x}) \\ \frac{\sqrt{2j}\,\epsilon}{E_j+m}\chi_j(q, b; \vec{x}) \end{bmatrix}, \tag{10b}$$

$$u_j^{(2)} = \left(\frac{E_j+m}{2m}\right)^{1/2} \begin{bmatrix} 0 \\ \chi_j(q, b; \vec{x}) \\ \frac{\sqrt{2j}\,\epsilon}{E_j+m}\chi_{j-1}(q, b; \vec{x}) \\ \frac{-q}{E_j+m}\chi_j(q, b; \vec{x}) \end{bmatrix}, \tag{10c}$$

and the scalar χ functions are given by

$$\chi_l(p, a; \vec{x}) = \frac{i^l}{(2^l l!)^{1/2}(\lambda^2\pi)^{1/4}} \frac{1}{L} \times \exp\left(\frac{1}{2\lambda^2}[iy(x-2a) - (x-a)^2] + ipz\right) \times H_j\left(\frac{x-a}{\lambda}\right), \quad l = 0, 1, 2, 3, \ldots . \tag{11}$$

The continuous parameters a and b in the above expressions are the initial and final x components of the orbit centers, which are eigenvalues for this choice of wavefunction. H_j in (11) is the jth Hermite polynomial, and the constant $\lambda = \epsilon^{-1}$ (in natural units).

In terms of these wave functions, the photon attenuation coefficients κ_1 and κ_2 (or κ_+ and κ_-) corresponding to the two choices of linear (or circular) polarization [Eq. (3)] are each given by expressions of the general form

$$\kappa(\omega, \theta) = n_0 L^3 \int dp\, \eta(p) \times \left(\frac{1}{T}\sum_{j=1}^{\infty} \int L\frac{dq}{2\pi} \int L\frac{db}{2\pi\lambda^2} \sum_{s=\pm 1} |S_{fi}|^2\right), \tag{12}$$

where

$$S_{fi} = ie \int d^4x \bar{\psi}_{\text{final}}(x) a^{\mu}(x) \gamma_{\mu} \psi_{\text{initial}}(x) . \tag{13}$$

The kinematical requirements already noted in Eqs. (6) and (7) are explicitly given by corresponding δ functions in the matrix element S_{fi}, which also contains the polarization dependence. Since $\bar{\psi}_f a^{\mu} \gamma_{\mu} \psi_i = \psi_f^{\dagger} a^k \alpha_k \psi_i$, the matrix element may immediately be rewritten in the form

$$S_{fi} = -ie \frac{1}{(2\omega L^3)^{1/2}} \left(\frac{m}{E_0}\right)^{1/2} \left(\frac{m}{E_j}\right)^{1/2} [2\pi\delta(E_j - E_0 - \omega)] \int d^3x e^{i\vec{k}\cdot\vec{x}} u_j^{\dagger(s)}(q, b; \vec{x}) \mathfrak{M} u_0(p, a; \vec{x}) , \tag{14}$$

where $\mathfrak{M}$ denotes one of the four polarization matrices

$$\mathfrak{M}_{(1,2)} = -\vec{\alpha}\cdot\hat{\epsilon}_{(1,2)} \quad \text{(linear)} , \tag{15a}$$

$$\mathfrak{M}_{(\pm)} = -\vec{\alpha}\cdot\hat{\epsilon}_{(\pm)} \quad \text{(circular)} . \tag{15b}$$

Note that $\mathfrak{M}_{(\pm)} = \mp(1/\sqrt{2})(\mathfrak{M}_{(1)} \pm i\mathfrak{M}_{(2)})$, a relation identical to that between the corresponding unit vectors.

The spatial integration in S_{fi} may be carried out using techniques explicitly discussed by Szegö.[16] The integrals occurring in this problem are special cases of the general form

$$\int d^3x e^{i\vec{k}\cdot\vec{x}} \chi_l(a, p; \vec{x}) \chi_m^*(b, q; \vec{x}) = \frac{1}{L^2} \frac{i^{l-m}}{(2^{l+m} l! m! \lambda^2\pi)^{1/2}} [2\pi\delta(p - q + \omega\cos\theta)] \left[2\pi\delta\left(\omega\sin\theta - \frac{a-b}{\lambda^2}\right)\right] \times \int dx H_l\left(\frac{x-a}{\lambda}\right) H_m\left(\frac{x-b}{\lambda}\right) \exp\left(-\frac{1}{2\lambda^2}[(x-a)^2 + (x-b)^2]\right) . \tag{16}$$

The factorization into δ functions and the one-dimensional integral in the form given above was the object of the choice of coordinate system (i.e., the restriction of the photon momentum vector $\vec{k}$ to the y-z plane).

The form of Eq. (16) prompts the definition of the quantity

$$\Omega_{lm} = \frac{i^{l-m}}{(2^{l+m} l! m! \lambda^2\pi)^{1/2}} \int_{-\infty}^{\infty} dx H_l\left(\frac{x-a}{\lambda}\right) H_m\left(\frac{x-b}{\lambda}\right) \exp\left(-\frac{1}{2\lambda^2}[(x-a)^2 + (x-b)^2]\right) . \tag{17}$$

The evaluation of (17) yields the rather compact result[2,16]

$$\Omega_{lm}=(-i)^{G-S}\left(\frac{S!}{G!}\right)^{1/2}e^{-Z/2}Z^{(G-S)/2}L_S^{G-S}(Z),\quad S=\min(l,m),\quad G=\max(l,m),\quad Z=\frac{1}{2}\left(\frac{a-b}{\lambda}\right)^2, \tag{18}$$

from which the symmetry property $\Omega_{lm}=\Omega_{ml}$ is immediately obvious. It is also apparent that Ω_{lm} is in fact a function of the dimensionless parameter Z. The generalized Laguerre polynomials $L_S^{G-S}(Z)$, which in the present problem $[S=\min(l,m)=0]$ are identically equal to unity, satisfy the definition and properties given in Abramowitz and Stegun.[17]

The algebra required to find S_{fi} is straightforward and will not be presented here. The evaluation of $|S_{fi}|^2$, involving the squared δ functions, are handled in the standard fashion as outlined in, for example, Bjorken and Drell.[15] However, careful attention must be given to the relative phases of $\Omega_{j,0}$ and $\Omega_{j-1,0}$.

Integrating $|S_{fi}|^2$ over the scattered-electron parameters q and b, and then summing over the final spin states as indicated in Eq. (12) yields

$$\begin{aligned}\int_L\frac{dq}{2\pi}\int_L\frac{db}{2\pi\lambda^2}\left(\sum_{s=1}^{2}|S_{fi}|^2\right)=\frac{e^2}{8\omega}\frac{2\pi T}{L^3}\delta(E_j-E_0-\omega)\frac{(E_0+m)(E_j+m)}{E_0E_j}\\ \times\Bigg\{|\Omega_{j,0}|^2D_1\left[\left(\frac{p}{E_0+m}+\frac{p+\omega\cos\theta}{E_j+m}\right)^2+\frac{2j\epsilon^2}{(E_j+m)^2}\right]\\ +|\Omega_{j-1,0}|^2D_2\left[\left(\frac{-p}{E_0+m}+\frac{p+\omega\cos\theta}{E_j+m}\right)^2+\frac{2j\epsilon^2}{(E_j+m)^2}\right]\\ -4|\Omega_{j,0}||\Omega_{j-1,0}|D_3\frac{\sqrt{2j}\,\epsilon}{E_j+m}\left(\frac{p}{E_0+m}\right)\Bigg\},\end{aligned} \tag{19}$$

where the three polarization-dependent coefficients D_1, D_2, D_3 in the bracketed expression are given for each case in the table below. Because of the two δ functions in Eq. (16), the momentum-conservation Eq. (6) is now enforced and in addition the parameter Z is henceforth restricted to be

$$Z=\frac{\omega^2\sin^2\theta}{2\epsilon^2}=\frac{1}{2}\left(\frac{\omega}{m}\right)^2\frac{B_{cr}}{B}\sin^2\theta\,. \tag{20}$$

Polarization:	(1)	(2)	(±)
D_1	$\sin^2\theta$	0	$\sin^2\theta/2$
D_2	$\cos^2\theta$	1	$(\cos\theta\pm1)^2/2$
D_3	$\sin\theta\cos\theta$	0	$\sin\theta(\cos\theta\pm1)/2$

From the general form of the attenuation coefficient [Eq. (12)] and the table, it is already possible to verify that $\kappa_1+\kappa_2=\kappa_++\kappa_-$, as expected. Furthermore, for $\theta=0$ (photons propagating parallel to the magnetic field), the relations

$$\kappa_1=\kappa_2=\tfrac{1}{2}\kappa_+\,,$$
$$\kappa_-=0$$

are found to hold. These properties will be discussed at greater length in Sec. IV below.

The remaining δ function in Eq. (19), which expresses energy conservation, may now be removed by the integration over the initial electron momentum distribution $\eta(p)$ in the expression for κ [Eq. (12)]. It is at this stage that the kinematics really enters into the problem, since for each final-state integer j only the set $\{p_i\}_j$ of zeros of the function $f(p)=E_j-E_0-\omega$ can contribute to the final result. That is, for each physical situation specified by given values of ω,θ,B, and each particular transition $0\to j$, only those electrons having certain discrete momentum values $\{p_i\}_j=p_{ij}$ can absorb the incident photon. In terms of these allowed momenta, it is possible to write the final expressions for each attenuation coefficient formally as

$$\begin{aligned}\kappa(\omega,\theta)=\frac{\pi^2\alpha\hbar^2c^2n_0}{(\hbar\omega)^2}e^{-Z}\sum_{j=1}^{\infty}\sum_i\eta(cp_{ij})\frac{2}{|E_0\cos\theta-cp_{ij}|}\\ \times\left(\frac{1}{j!}Z^jD_1[E_0E_j-m^2c^4+cp_{ij}(cp_{ij}+\hbar\omega\cos\theta)]\right.\\ \left.+\frac{1}{(j-1)!}Z^{j-1}D_2[E_0E_j-m^2c^4-cp_{ij}(cp_{ij}+\hbar\omega\cos\theta)]-\frac{2\sqrt{2}}{(j-1)!}Z^{j-1/2}D_3\epsilon cp_{ij}\right).\end{aligned} \tag{21}$$

Here conventional (cgs Gaussian) units have been reinstated for convenience, so that κ has the dimension cm^{-1}. Thus the problem has been reduced to that of finding the discrete allowed momenta p_{ij} for each j.

III. KINEMATICAL REQUIREMENTS AND ALLOWED MOMENTA

The momentum-conservation Eq. (6) may be incorporated into Eq. (7) for the energy, and the result may be squared to give

$$(p^2+m^2)^{1/2}=p\cos\theta+\zeta_j \ , \tag{22a}$$

where

$$\zeta_j=j\frac{B}{B_{cr}}\frac{m^2}{\omega}-\frac{\omega}{2}\sin^2\theta \ . \tag{22b}$$

It is possible to search for solutions of (22) geometrically by plotting the two functions $f_1(p)=(p^2+m^2)^{1/2}$ and $f_2(p)=p\cos\theta+\zeta_j$ and finding their points of intersection. It is immediately obvious from this geometrical method that since $|\cos\theta|\leq 1$, so solution exists if $\zeta_j<0$. This is an important observation, since to proceed further it is necessary to square Eq. (22a) a second time, obtaining the quadratic expression

$$\sin^2\theta p^2-2\zeta_j\cos\theta p+(m^2-\zeta_j{}^2)=0 \ . \tag{23}$$

The only pitfall in using the latter equation to find the desired $\{p_i\}_j$ is that real solutions are obtained whenever $\zeta_j{}^2\geq m^2\sin^2\theta$, whereas the necessary and sufficient requirement for solutions of Eq. (22) to exist is that $\zeta_j\geq m\sin\theta$.

The case $\zeta_j=m\sin\theta>0$ gives exactly one solution p_j for each j (in the geometrical picture, the two curves are tangent at this point). However, for the particular values of ω, θ, and B which fulfill this condition, the absorption coefficients κ for all polarizations become singular. This behavior arises from the vanishing of $|d(E_j-E_0-\omega)/dp|$, which is contained in the denominator of Eq. (21) for κ after the last integration involving $\delta(E_j-E_0-\omega)$. For fixed field strengths, the condition $\zeta_j=m\sin\theta$ can be solved to give the discrete frequencies

$$\omega_j=\frac{m[(1+2jB/B_{cr})^{1/2}-1]}{\sin\theta} \tag{24}$$

at which the singularities occur.

If $\sin\theta=0$, the quadratic equation (23) is reduced to a linear equation for p. Thus there is again only one solution, which in this instance is given by

$$p_j=\frac{m^2-\zeta_j{}^2}{2\zeta_j} \ . \tag{25}$$

However, in this case there is no singularity in the attenuation coefficients, since $|d(E_j-E_0-\omega)/dp|$ does not vanish for finite p. For later use it is worthwhile to make note of the limiting cases

$$p_j\to\frac{m^2}{2\zeta_j} \ , \quad \zeta_j\ll m$$

$$p_j\to-\frac{\zeta_j}{2} \ , \quad \zeta_j\gg m \ .$$

For the remaining possibility, $\zeta_j>m\sin\theta>0$, there are two solutions which are just the roots of (23), namely,

$$p_j^{\pm}=\frac{\zeta_j\cos\theta\pm(\zeta_j{}^2-m^2\sin^2\theta)^{1/2}}{\sin^2\theta} \ . \tag{26}$$

It is of particular interest to examine the behavior of these solutions in the limit $\zeta_j\gg m\sin\theta$, for which

$$p_+\sim\frac{\zeta_j}{1-\cos\theta}-\frac{m^2}{2\zeta_j} \ , \tag{27a}$$

$$p_-\sim\frac{-\zeta_j}{1+\cos\theta}+\frac{m^2}{2\zeta_j} \ . \tag{27b}$$

Under the more restrictive assumption $\zeta_j\gg m$, the solutions take the especially simple forms

$$p_+\sim\frac{\zeta_j}{1-\cos\theta} \ , \tag{28a}$$

$$p_-\sim\frac{-\zeta_j}{1+\cos\theta} \ . \tag{28b}$$

In the geometrical picture mentioned above, these last solutions are just the intercepts of the line $f_2(p)=p\cos\theta+\zeta_j$ with the asymptotes $a_\pm(p)=\pm p$ of the curve $f_1(p)=(p^2+m^2)^{1/2}$.

IV. LIMITING FORMS OF THE ATTENUATION COEFFICIENTS

The equations for the allowed momenta derived in the previous section complete the general solution (21) for the first-order attenuation coefficients, which (within the limits of the perturbation theory approach) is valid for arbitrary values of ω, θ, and B. Unfortunately the latter expression is in general rather cumbersome, and its form does not immediately provide much insight about the properties of each κ. However, for the physically interesting cases of nearly parallel propagation and/or low frequencies, it is possible to establish several (partially independent) criteria which may reduce the number of terms appearing in (21) as follows:

A. Behavior at small angles

(1) If $\sin\theta\ll(B/B_{cr})^{1/2}(m/\omega)$, then the parameter Z [Eq. (20)] becomes much less than unity and $\exp(-Z)\sim 1$ in Eq. (21). In addition, the jth term in the summation in (21) is roughly a factor $Z/\sqrt{j}$ smaller than the preceding term. Hence, it is possible in the limit of small Z to neglect all but the first kinetically allowed term, which for field strengths of the same order as B_{cr} or less is always $j=1$.

(2) Of the pair of momentum solutions $p_\pm$ for nonzero θ in Eq. (26), it is p_- which tends to the

solution (25) for parallel propagation as $\theta \to 0$, whereas p_+ goes to infinity in the same limit. Thus, if $\eta(p)$ falls off rapidly enough for large positive p, only the terms involving p_- contribute to each κ.

(3) As $\theta \to 0$, both the first and third terms within the brackets in (21) go to zero, whereas the middle term approaches a finite value proportional to $(B/B_{cr})m^2$. If in addition $\eta(p_+) \sim 0$, then again only the p_- contribution remains, for which the factor in the denominator

$$|E_0 \cos\theta - p_-| \to E_0 + |p_-| \sim \zeta_1 = \frac{B}{B_{cr}} \frac{m^2}{\omega} .$$

For the case $\theta = 0$ exactly, all the above conditions apply and the attenuation coefficients then have the especially simple forms

$$\kappa_{(1)} = \kappa_{(2)} = \tfrac{1}{2}\kappa_{(+)} = \frac{2\pi^2 \alpha \hbar^2 c^2 n_0}{(\hbar\omega)} \eta[cp(\omega)] , \qquad (29a)$$

$$\kappa_{(-)} = 0 . \qquad (29b)$$

Moreover, it is true in general that each κ approaches the above limiting values continuously as $\theta \to 0$.

On the other hand, it must be stressed that for arbitrary choices of ω, B, and the momentum distribution $\eta(p)$, κ may be an extremely sensitive function of θ at small but finite angles. In fact, for a given nonzero $\theta \ll 1$ it may still turn out that none of the above criteria are fulfilled, and only the exact form of (21) can give reliable results [which may differ significantly from the limits (29) above]. However, it is generally possible to write simpler expressions for κ for nonzero θ if additional low-frequency limits may be imposed, as will be discussed below.

B. Low frequencies

(1) The first criterion mentioned in part A above is properly viewed either as a limit of small angles or of low frequencies. Thus if

$$\omega \ll \left(\frac{B}{B_{cr}}\right)^{1/2} \frac{m}{\sin\theta}$$

for arbitrary θ, it is again true that $Z \ll 1$ and only the first allowed j term in (21) need be retained.

(2) If $\omega \ll (B/B_{cr})m$ [which for all $B < B_{cr}$ is a more restrictive low-frequency condition than (1) above], then again only the $j = 1$ term is significant. Furthermore, from Eq. (22b) it is seen that

$$\zeta_1 \sim \frac{B}{B_{cr}} \frac{m^2}{\omega} \gg m .$$

Thus the simple expressions (28) for the allowed momenta apply for nonzero θ.

It also follows that $|q| = |p + \omega\cos\theta| \sim |p| \gg m$, so that q and p have the same sign. This fact and the use of the approximations

$$E_0 \sim |p_\pm| \left(1 + \frac{m^2}{2p_\pm^2}\right) ,$$

$$E_1 \sim |q_\pm| \left(1 + \frac{m^2 + 2\epsilon^2}{2q_\pm^2}\right) ,$$

lead to the results

$$E_0 E_1 - m^2 + pq \sim 2p_\pm^2 \sim \frac{2\zeta_1^2}{(1 \mp \cos\theta)^2} ,$$

$$E_0 E_1 - m^2 - pq \sim \epsilon^2 = \frac{B}{B_{cr}} m^2 ,$$

for the corresponding factors appearing in (21).

The factors $|E_0\cos\theta - p_\pm|$ in the denominators of (21) present no problems if $\eta(p_+) \sim 0$, since then $|E_0\cos\theta - p_-| \sim \zeta_1$ is the only term which need be considered. If $\eta(p_+)$ cannot be neglected, however, it is then necessary to impose the additional restriction $\theta \gg m/p_+$, so that $|E_0\cos\theta - p_+| \sim \zeta_1$ also. In either case, it is then finally possible to combine the above results and reduce (21) to the compact forms

$$\kappa_{(1)} \sim \kappa_{(2)} \sim \frac{2\pi^2 \alpha \hbar^2 c^2 n_0}{(\hbar\omega)} \sum_\pm \eta(cp_\pm) , \qquad (30a)$$

$$\kappa_{(\pm)} \sim \frac{4\pi^2 \alpha \hbar^2 c^2 n_0}{(\hbar\omega)} \eta(cp_\mp) . \qquad (30b)$$

These expressions are seen to agree with Eq. (29) for the case $\theta = 0$ (and arbitrary ω), since p_+ tends to infinity and $\eta(p_+)$ necessarily vanishes as $\theta \to 0$. Moreover, in the present low-frequency limit, the expressions (30) are valid at all θ for which either the condition $\theta \gg m/p_+$ is satisfied or $\eta(p_+)$ effectively vanishes. If neither of these conditions is fulfilled, then the exact form (21) should again be used instead of (30).

V. APPLICATIONS

In the present section a few specific choices for the electron momentum distribution $\eta(p)$ will be postulated in order to demonstrate several interesting aspects of the first-order absorption process. It should be emphasized that the examples used here are not all equally justifiable on physical grounds, although at least some of the forms for $\eta(p)$ given below are directly motivated by recent models of the electron plasmas in pulsar magnetospheres.

In general, it is true that the first-order absorption effect becomes significant over a wider range of frequencies (and incident angles) as $\eta(p)$ spans a greater range of momenta, so that a broad spectrum of electrons is available to fulfill the differing kinematical requirements correspond-

ing to variations in ω and θ. (The effects of spatial variations in B must also be considered in applications to pulsar magnetospheres, although for present purposes it is convenient to maintain the arbitrary point of view that B is in each case a fixed parameter.) Both to demonstrate the "smeared-out" appearance of $\kappa(\omega, \theta)$ which results from a broad momentum distribution, and to illustrate the occurrence of the singular absorption lines at the discrete frequencies given by Eq. (24), the first choice of $\eta(p)$ will be the half-Gaussian form

$$\eta(p) = 0, \quad p < 0$$
$$= \frac{2}{\sqrt{\pi}\, p_c} \exp\left(-\frac{p^2}{p_c{}^2}\right), \quad p \geq 0 \tag{31}$$

where p_c will be arbitrarily set at 1 GeV for definiteness. This specific choice of p_c is not likely to be very reasonable for a thermal or evaporation spectrum (because of the extremely high implied temperature, namely, $T \sim 10^{13}$ K), but it does provide an especially simple example of a highly broadened distribution (some more complicated form of which may conceivably arise on other physical grounds, such as electrostatic acceleration with nonlinear space-charge effects).

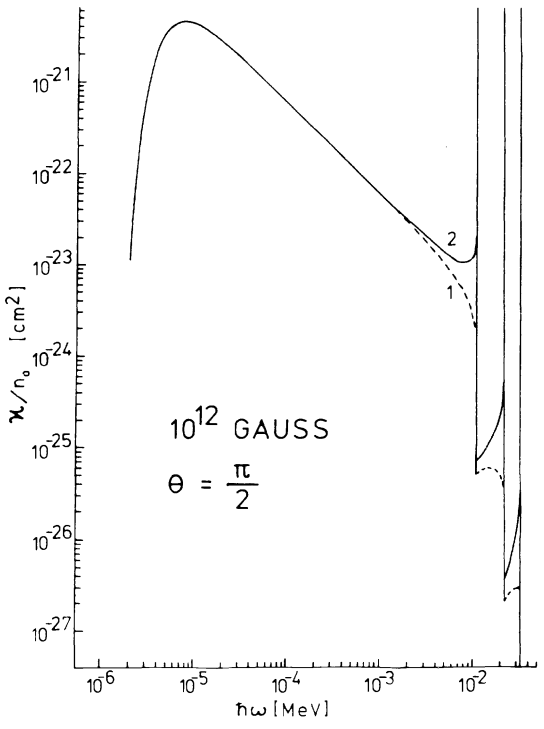

FIG. 3. Specific attenuation coefficients κ/n_0 vs photon energy for $\theta = \pi/2$, corresponding to the half-Gaussian electron momentum distribution given by Eq. (31), with $p_c = 1$ GeV. The field strength is here chosen to be 10^{12} G. The curves shown are for the two linear polarizations specified by Eq. (3). The high-energy portion of the graph displays the lowest critical frequencies at which singularities occur for both polarizations, while the smooth rollover at low energies reflects the drop in the electron spectrum above 1 GeV. The broad portion over which it is almost inversely proportional to ω (corresponding to the flat part of the electron spectrum) satisfies the approximations (28a) and (30a).

The specific attenuation coefficients κ/n_0 corresponding to the above form of $\eta(p)$ and a field strength $B = 10^{12}$ G are plotted in Fig. 3 as a function of frequency, at first for $\theta = \pi/2$ only. (Note that κ/n_0 has the dimensions of a cross section.) The exact solution (21) for each κ was used to obtain the above graph, although it can immediately be seen that in the range for which $\omega \ll (B/B_{cr})m$, κ satisfies the approximate Eq. (30). Above this range the singularities at the lowest critical frequencies $\omega_j(\theta, B)$ as given by Eq. (24) are clearly evident, and are separated by a narrowing, stepwise decreasing sequence of continuous segments.

The influence of the specific form of $\eta(p)$ in Fig. 3 is most obvious in the low-frequency range (well below the first critical frequency). As would be expected from Eq. (30), κ is almost inversely proportional to ω over the broad range for which $\eta(p_+)$ is nearly constant. [The p_- solutions, being always negative in this example, do not appear for this form of $\eta(p)$.] The low-frequency cutoff in κ, whose location is dependent on field strength as well as incident angle, corresponds to the eventual drop in $\eta(p_+)$ as p_+ increases beyond the characteristic value p_c.

Variations of the above graph are shown in Figs. 4, 5, and 6, which are intended to illustrate the dependence of κ on the angle of incidence as well as different choices for the ambient field strenghts (at fixed angles). Each of these graphs has a number of points of technical interest, as in the case of the small-angle behavior in Fig. 5, which is in part due to the asymmetry of $\eta(p)$ in this example and the behavior of the momentum solutions $p_\pm$ as $\theta \to 0$. Technical features of this type will not be discussed in detail. However, one point which is worth noting is the behavior of κ as B is reduced, as shown in Fig. 6. It is apparent that the low-frequency end of κ (the cutoff region) "slides" backward and upward along a fixed line proportional to ω^{-1} as B is decreased, although for all nonzero θ the discrete singularities also move backward to lower values of ω:

$$\omega_j \to j \frac{B}{B_{cr}} \frac{m}{\sin\theta} \text{ as } \frac{B}{B_{cr}} \to 0 .$$

In fact, as B goes to zero for any fixed $\theta > 0$, the entire structure of κ is compressed into a line of infinite height at $\omega = 0$ (corresponding to an infinite

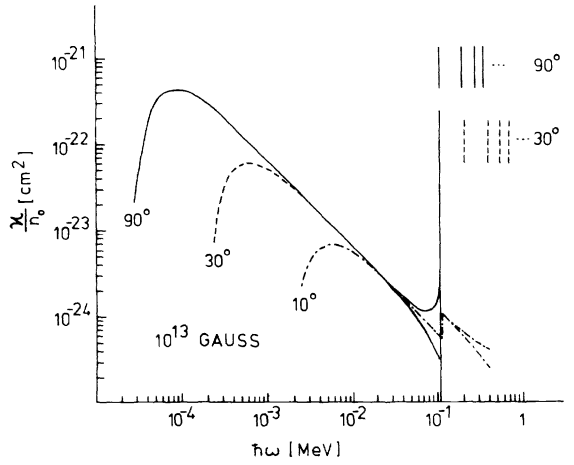

FIG. 4. The behavior of κ/n_0 vs ω at different angles of incidence for a fixed field strength, here chosen to be 10^{13} G. The assumed electron distribution is identical to that for Fig. 3. For 90° and 30° only the low-energy portions of the curves are shown (below the first critical frequency for 90°), although the upper right-hand corner indicates the shift of all the singularities toward higher frequencies as θ is decreased [see Eq. (24)]. The critical frequencies for 10° are not shown. However, the latter curve is extended above 0.1 MeV to include an abrupt increase by a factor of 2, which occurs when both the momentum solutions (26) become positive and contribute to the absorption [See Eq. (30a)].

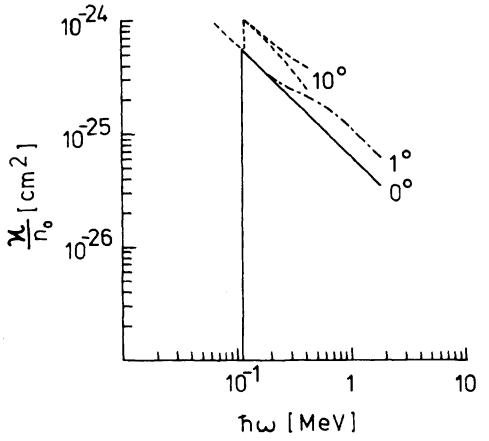

FIG. 5. Continuation of Fig. 4 to smaller angles. The factor-of-2 increase in κ/n_0 for 10° is also shown here. This may be compared with the gradual increase for 1° incidence, the difference being that for increasing frequency, the p_+ contribution is the first to appear in the former case and p_- in the latter case. For $\theta = 0$ there is only one finite-momentum solution, which is increasing with photon energy.

absorption probability for photons of zero frequency). However, this is tantamount to saying that no absorption is possible for any real photon of frequency $\omega > 0$, as expected for field-free space. The same is of course true for the case $\theta = 0$ exactly, since then the allowed momenta [Eq. (25)] are always infinite for all $\omega > 0$ even though there are no finite critical frequencies.

The second example for $\eta(p)$ is chosen to illustrate the opposite extreme of a sharply peaked distribution. This case will be of direct relevance for pulsars if some types of magnetospheric plasma instabilities can act as bunching mechanisms to produce localized "clouds" of (positive or negative) electrons moving with sharply defined energies, as a number of authors have suggested.[7,8] Coherent radiation from such electron clouds has in fact been pictured as the source of the observed radio emission.

For present purposes, the momentum distribution of a typical electron cloud may be approximated by the full Gaussian form

$$\eta(p) = \frac{1}{\sqrt{\pi}\, p_c} \exp\left(-\frac{(p-p_0)^2}{{p_c}^2}\right) , \qquad (32)$$

where it is postulated that the average momentum $p_0 \gg p_c$. Since it appears likely that ultrarelativistic electrons would be required to account for the pulsar radiation mechanism, the additional condition $p_0 \gg m$ will also be imposed.

In the context of this example, it is convenient to consider one of the allowed momentum solutions $p_\pm$ in Eq. (26) as coinciding *a priori* with a chosen p_0, and then to determine accordingly what frequency range can be absorbed for any given angle of incidence. Here it will be sufficient to consider only the simplest cases of physical interest, so it will be assumed that $p_+ = p_0$ and θ will be restricted to finite values such that $p_0(1 - \cos\theta) \gg m$. Then from Eq. (28), the range of frequencies subject to absorption is approximately centered on the value

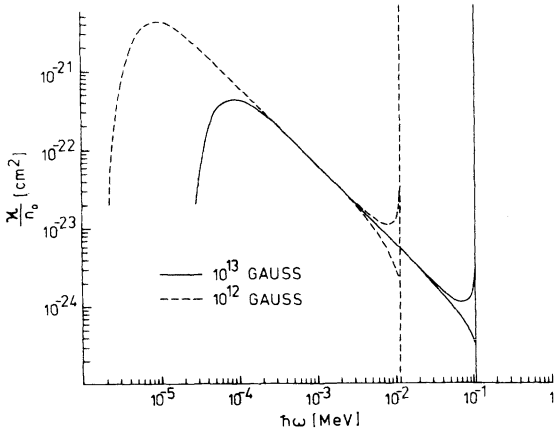

FIG. 6. Behavior of κ/n_0 for different field strengths, at fixed angle of incidence (here 90°). See discussion in Sec. V.

$$\omega_0 \sim \frac{B}{B_{cr}} \frac{m^2}{p_0(1-\cos\theta)} \ll \frac{B}{B_{cr}} m \,. \tag{33}$$

Figure 7 shows a plot of κ vs ω for the specific choices $p_0 = 10^4$ MeV, $p_c = 10^3$ MeV, $\theta = 10°$, and a field strength $B = 10^6$ G (which should be a reasonable value for the light cylinder region of the Crab pulsar or the intermediate zones of slower pulsars). The choices of p_0 and θ were here contrived to result in absorption around 1 GHz, but appear sufficiently reasonable to suggest the importance of first-order absorption at radio frequencies.

This graph also illustrates an important aspect of the absorption effect which holds whenever the low-frequency approximation (33) above is valid, namely, that the relative bandwidth of affected frequencies $\delta\omega/\omega$ is roughly as narrow as the effective width of the electron momentum distribution $\delta p/p$. This property holds here because $\omega \propto p^{-1}$, which for large p_0 remains true for all $\theta \gg (m/p_0)^{1/2}$.

One further remark seems appropriate in connection with the above example: It is interesting to speculate about the behavior of large numbers of such localized electron clouds moving along magnetospheric field lines with various average momenta p_0, in the case for which the cloud dimensions and/or densities are sufficient to make first-order absorption significant. This picture may well hint at a partial explanation for the extremely complicated (and variable) radio pulse

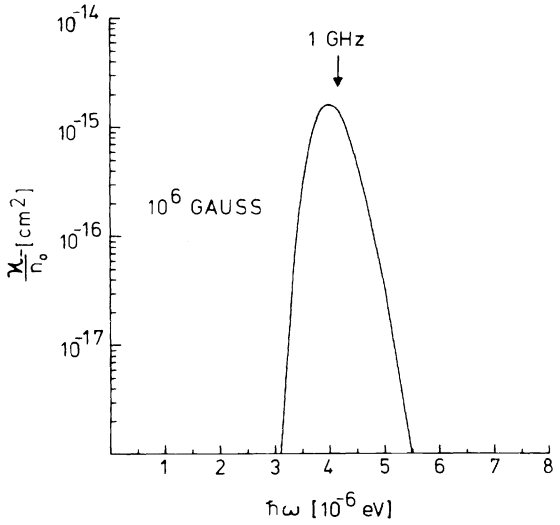

FIG. 7. Absorption at radio frequencies by a relativistic bunch of electrons in a megagauss field. A "typical" incident angle of 10° is assumed for definiteness. The postulated electron distribution has a full Gaussian shape [see Eq. (32)], with $p_0 = 9.7$ GeV and $p_c = 1.0$ GeV, these values being chosen to result in absorption at 1 GHz.

structure observed from most pulsars. Complex amplitude-time and amplitude-frequency dependences (often much sharper than might be expected from incoherent emission mechanisms alone) would be essential features of the net radiation pattern from numerous electron clouds, each capable of both emitting radiation and absorbing multiple frequency bands of the emission spectra from other clouds. (The observed polarization effects would demand a more specific picture, but might be the result either of the emission mechanism, whether curvature or synchrotron radiation, or of the simultaneous presence of both positive and negative electrons in the clouds.)

A third example for $\eta(p)$, of interest in connection with pulsating x-ray sources, would be given by choosing a mildly relativistic, negative value for p_0 (typically $cp_0 \lesssim 300$ keV) in the Gaussian form (32). Here again, depending on the momentum dispersion, polarization-dependent absorption features roughly similar in appearance to Fig. 7 would be obtained, except that for $B \sim 10^{12}$ G, the absorption would be centered in the hard x-ray regime. The question of radiative transfer in pulsating x-ray sources, however, is of sufficient interest in itself to warrant a more detailed treatment of this type of example than can be attempted here. For reasons of space, this task must be reserved for a separate paper.

VI. COMPARISON OF FIRST-ORDER ABSORPTION AND COMPTON SCATTERING: VALIDITY OF THE FIRST-ORDER THEORY

It was already mentioned in the Introduction that the derivation of the first-order attenuation coefficients given above must be revised for the case of high electron densities or low frequencies, for which it may become improper to use the vacuum radiation field satisfying the condition $k_\mu k^\mu = 0$. On the other hand, the dispersive behavior of the radiation field in dense plasmas is essentially a technical problem which does not bring into question the validity of the general first-order perturbation theory approach outlined above.

The extrapolation to the opposite limit of extremely low densities, however, requires a fundamental change in viewpoint. In fact, the first-order result (21) itself becomes a poor approximation as soon as the ensemble of electrons which may interact with the photon can no longer be described by a continuous distribution function such as that used here, $f_0(\mathbf{p}, \vec{\mathbf{x}}, t) = n_0\eta(p)$. To analyze this limit, in which the effect of discrete numbers of electrons becomes apparent, the precise relation of the (second-order) Compton effect to the first-order absorption process must be made more

explicit.

The approach to low densities can be visualized in qualitative terms as follows: As n_0 is decreased, the momentum distribution $\eta(p)$ is effectively resolved into a sum of δ functions in momentum space (assuming the particle momenta are all rather sharply defined):

$$\eta(p) \to \frac{1}{N} \sum_{i=1}^{N} \delta(p-p_i).$$

In second order, each electron can undergo (magnetic) Compton scattering as shown in Figs. 2(b), 2(c) with an incident photon of arbitrary energy ω and propagation angle θ, so that the attenuation coefficient due to the presence of even a single electron is a continuous, smeared-out function of these variables (as opposed to the δ-function behavior of the first-order approximation). However, for those pairs of ω and θ which happen to satisfy the kinematical requirements (6) and (7) for first-order absorption, the Compton cross section for one polarization displays an extremely sharp resonance, which can be shown to arise only from the "uncrossed" diagram 2(b). In precisely these cases the electron propagator acquires an extremely long lifetime and effectively achieves the status of a "real" particle, which eventually (i.e., after measurable times) undergoes magnetic bremsstrahlung. Thus, at the resonance, diagram 2(b) may be viewed as a sequence of the two independent first-order diagrams 2(a) and 1(a).

The finite transition rate for synchrotron emission is just the mechanism which keeps the Compton resonance finite and determines both its height and its natural width (in a manner completely analogous to radiation damping in atomic transitions: see, for example, Sakurai[18]). A short derivation of the synchrotron transition rate (inverse of the mean lifetime τ) for the two cases of principal interest here, namely,

$$|j=1, s=1\rangle \to |j=0\rangle + \gamma \ ,$$

$$|j=1, s=-1\rangle \to |j=0\rangle + \gamma \ ,$$

is presented in the Appendix. For nonrelativistic electrons ($p \sim 0$) and $B/B_{cr} \ll 1$, τ has the simple forms

$$\tau_{s=1} \sim \frac{3}{2} \frac{\hbar}{\alpha} \left(\frac{B_{cr}}{B}\right)^3 \frac{1}{mc^2} \ , \tag{34a}$$

$$\tau_{s=-1} \sim \frac{3}{4} \frac{\hbar}{\alpha} \left(\frac{B_{cr}}{B}\right)^2 \frac{1}{mc^2} \ll \tau_{s=1} \ . \tag{34b}$$

As might be expected, for Lorentz frames in which $p \neq 0$ the above values are each increased by the factor $\gamma_{\parallel} = (p^2 + m^2 + 2\epsilon^2)^{1/2}/m$.

A simple illustration of the damping effect of τ on the Compton resonance is provided by noting that the low-energy (Thomson) limit for parallel propagation ($\theta = 0$) derived by Canuto *et al.*[19] should be modified as follows:

$$\frac{\sigma_{\pm}}{\sigma_{th}} = \frac{\omega^2}{(\omega \mp \omega_H)^2} \to \frac{\omega^2}{(\omega \mp \omega_H)^2 + \Gamma^2/4\hbar^2} \ , \tag{35}$$

where

$$\sigma_{th} = \frac{8\pi}{3}\left(\frac{e^2}{mc^2}\right)^2, \quad \Gamma = \frac{\hbar}{\tau} \ ,$$

and

$$\hbar\omega_H = \frac{e\hbar}{mc} B = \frac{B}{B_{cr}} mc^2 \ .$$

The resonance is obviously associated with σ_+ (the extraordinary mode), and is evidently extremely high for all field strength comparable to or less than B_{cr}. The "nonresonant" portion of σ_+/σ_{th} is plotted vs frequency in Fig. 8 to suggest the sharpness of the peak (for $B < B_{cr}$ the natural width Γ is not observable in this graph).

The finite height and width of the resonance which appear in second order have a direct bearing on the validity of the first-order approximation derived in this work, as may be inferred immediately from the analogous situation for radiation damping in atomic transitions.[18] In particular, it is essential that the time in which the photon (in realistic terms, a radiation pulse of finite duration) can interact with the electrons must be short

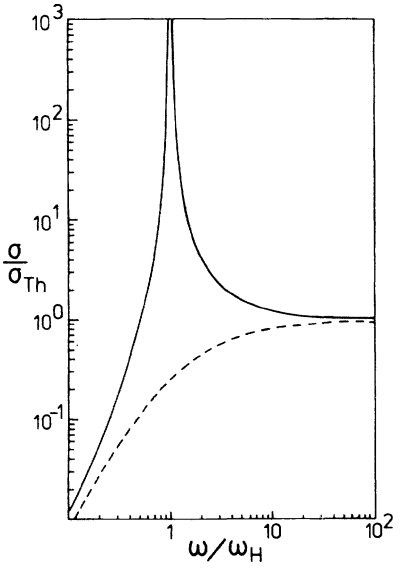

FIG. 8. Behavior of Thomson scattering cross sections for the case of parallel propagation. The solid (dashed) line refers to photons of photons of positive (negative) helicity. The absorptive resonance for positive-helicity photons, whose peak is dependent on field strength (see Appendix), occurs at the cyclotron frequency $\omega_H = (B/B_{cr})\, mc^2$ for electrons at rest.

compared with the lifetimes of the "excited" electron states: otherwise, the absorption and reemission cannot be treated as two independent quantum-mechanical processes, and the first-order approximation must break down. However, the interaction time is related by the uncertainty principle to the energy resolution of the photon beam, so that the validity of the first-order approach in effect requires that

$$\Delta(\hbar\omega) \gg \Gamma(B) \ . \tag{36}$$

This condition is not unreasonably stringent and can be satisfied in many physical applications, but indicates that some caution is necessary at low (radio) frequencies and high field strengths, $B \lesssim B_{cr}$.

On the other hand, the above criterion (36) is not sufficient by itself to determine whether the first-order attenuation coefficient (21) is a good approximation. This may be seen by a further examination of the second-order picture, in which the Compton cross sections due to all the individual electrons which can scatter the incident photon must be superimposed to give the resultant attenuation coefficients. But now it must be realized that the location of each Compton resonance (considered as a function of frequency and/or angle) depends on the individual electron momentum p_i. Thus, for example, the cross section for parallel propagation in Fig. 8 is shifted to higher frequencies for $p>0$, so that the resonance occurs at $\omega > \omega_H$. Hence, for an ensemble of electrons, the amount of overlap in the individual cross sections becomes a critical question.

In this context it is highly instructive to pursue the example of parallel propagation somewhat further, especially since in this case the use of Lorentz transformations permits the immediate generalization of (35) to an electron with any nonzero p. Thus if $v=p/E_0$, $\gamma=E_0/m$, and primed quantities are understood to refer to the electron rest frame, then

$$\omega' = \gamma(1-v)\omega \ ,$$

$$n_0' = \frac{1}{\gamma} n_0 \ ,$$

$$\kappa' = (\lambda')^{-1} = \frac{\kappa}{\gamma(1-v)} \ .$$

It follows immediately that

$$\frac{\kappa}{n_0} = (1-v)\sigma' \ ,$$

where

$$\sigma_{\pm}' = \frac{\kappa_{\pm}'}{n_0'} = \sigma_{th} \frac{\omega'^2}{(\omega' \mp \omega_H)^2 + \Gamma^2/4} \ .$$

It is further possible in this case to obtain the average cross section $\langle\sigma_+\rangle$ for the resonant polarization, and hence the resultant attenuation coefficient $\langle\kappa_+\rangle$, for the same distribution of electrons (2) which was assumed in the derivation of the first-order attenuation coefficients:

$$\langle\sigma_+\rangle = \frac{\langle\kappa_+\rangle}{n_0} = \int dp\eta(p) \frac{\kappa_+(\omega,p)}{n_0}$$

$$= \sigma_{th} \int dp\eta(p) \frac{\omega'^2(1-v)}{[(\omega'-\omega_H)^2+\Gamma^2/4]}$$

$$= \sigma_{th} \int dp\eta(p) \frac{\omega^2(1-p/E)}{\left\{\left[\omega - \left(\frac{m}{E-p}\right)\omega_H\right]^2 + \frac{\Gamma^2}{4}\left(\frac{m}{E-p}\right)^2\right\}} \ . \tag{37}$$

Now at this point it must be noted that these last expressions are supposed to describe the same physics, to second order, as the corresponding first-order solution (29a). Whether this is the case, however, depends not only on whether Γ is sufficiently small, but also on the smoothness of the distribution $\eta(p)$ (or equivalently, on the amount of overlap in the cross sections due to the individual electrons). The same assumptions implicit in the framework of the first-order approximation would also imply here that a large number of the resonance peaks must overlap on a scale comparable with the natural width of each peak. If this restriction does not hold, then the final integration involving the energy δ function $\delta(E_j - E_0 - \omega)$, which resulted in Eq. (21), is not generally valid. In other words, the first-order treatment must break down as the density n_0 is lowered to the point at which the individual peaks move apart from each other and can be separately resolved.

On the other hand, for the continuum limit in which $\eta(p)$ may be used, the first- and second-order descriptions show good agreement. Thus, if the main contribution to the integral (34) is confined to the natural width Γ of the peak and if $\eta(p)$ does not vary appreciably over this narrow range, then it is possible to write

$$\frac{\bar{\kappa}_+}{n_0} = \sigma_{th} \frac{m}{\omega} \int d\omega' \eta(p(\omega')) \frac{\omega'^2}{[(\omega'-\omega_H)^2+\Gamma^2/4]}$$

$$\sim \sigma_{th} \eta(p(\omega_H)) \frac{4\omega_H^2}{\Gamma^2} \Gamma \frac{m}{\omega} \ . \tag{38}$$

But since (in natural units)

$$\sigma_{th} = \frac{8\pi}{3} \frac{\alpha^2}{m^2}$$

and

$$\Gamma = \frac{4}{3}\alpha\frac{\omega_H^2}{m},$$

$$\frac{\tilde{\kappa}_+}{n_0} \sim \frac{8\pi\alpha\hbar^2c^2}{\hbar\omega}\eta(cp). \tag{39}$$

The discrepancy between this crude integration and the first-order result is just $\pi/2$, which should perhaps be considered somewhat fortunate. Nevertheless, the point of this example, namely, the requirement of a quasicontinuous electron distribution, clearly extends to more general cases for which $\theta > 0$.

A rough test for the smoothness of the electron distribution is provided in the case of simple forms of $\eta(p)$ with effective width δp by checking for the inequality

$$\frac{\delta p}{n_0\delta^3 x} \ll \frac{1}{\hbar}\Gamma\frac{dp}{d\omega}, \tag{40}$$

where $\delta^3 x$ is the volume within which the photons (i.e., pulse of radiation) are confined by the emitting mechanism (so that it is impossible in principle to determine which of the electrons within $\delta^3 x$ interacts with any photon). This volume must in turn be defined according to the realistic energy and angular resolutions expected for the radiation pulse.

If both of the criteria (36) and (40) above hold, then the first-order expression (21) for κ is likely to be a good approximation. In other cases, more reliable values might be obtained from integral second-order expressions similar to (37).

VII. DISCUSSION: SUGGESTED ASTROPHYSICAL APPLICATIONS

The principal conclusion to be drawn from this work is that the absorption of radiation by electrons in high magnetic fields, which must be considered one of the simplest elementary processes allowed in quantum perturbation theory, nevertheless, may very well introduce a number of striking and rather complex features into the physics of radiative transport in neutron-star (or while dwarf) magnetospheres. It has been demonstrated explicitly that the absorption process, to an extent even greater than for Compton scattering[19-21] in magnetic fields, is characterized by a complicated selectivity in frequencies and polarizations which is strongly dependent on both the momentum distribution and charge composition of the electron plasma.

At the same time, the present work has been restricted primarily to the general physical aspects of the absorption process and the validity of its first-order description. For reasons of space it must be reserved for separate investigations to apply the above results in a detailed way to specific astrophysical applications. However, two cases of particular interest may be briefly mentioned here to further emphasize the relevance of this process.

Several authors of recent pulsar models[7,8] have suggested that two-stream instabilities or other mechanisms can produce localized bunches of electrons which stream outward along open magnetic field lines between the surface of the neutron star and the light cylinder. The transport of radiation (which may be emitted initially because of the curvature of the field lines) through a large number of electron bunches should involve (in addition to cascade effects) a repeated sequence of first-order absorption and re-emission processes as well as (nonresonant) Compton scattering. The capability of the emerging radiation in such models to explain the observed (probably coherent) radio emission characteristics must be carefully investigated. In this context, the obvious possibility of first-order absorption as a pumping mechanism for maser emission should not be ignored.

Absorption by a distribution of electrons may also be responsible for observed spectral features in the pulsed x-ray emission from objects such as Her X-1.[11,22,23] One previous attempt[24] to explain the remarkably steep cutoff in the Her X-1 spectrum between 20–30 keV was based on the assumption that the electrons above the polar cap region of the star become optically thick at frequencies well below ω_H [cf. Eq. (35), and Fig. 8]. However, it would be interesting to investigate the alternative possibility that the observed cutoff is a moderately broad-band first-order absorption effect due to a thermal distribution of electrons. In this context the re-emerging feature suggestive of an emission line around 53 keV, which has very recently been reported,[11] may be quite significant.

One further outstanding question of more general interest should be mentioned in conclusion: It would be useful to investigate the relation of the quantum-mechanical treatment of the absorption process to the well-known classical formulas for synchrotron reabsorption (see, for example, Ginzburg and Syrovatskii[25]), derived under the combined assumptions of low field strength, isotropic electron distributions (which imply a quasicontinuous population of higher orbital states extending to enormous values of j), and radiative equilibrium. It seems likely that a more elaborate quantum treatment, starting from electron distribution functions which allow the population of many orbital levels, could provide valuable generalizations of the classical description of synchrotron reabsorption.

APPENDIX: LIFETIMES OF THE FIRST EXCITED STATES IN A UNIFORM MAGNETIC FIELD

Let E_1, q and b denote the initial energy, longitudinal momentum, and x eigenvalue of an electron in a uniform field $B = Bz$. The particle may be in either of the two spin states corresponding to the quantum number $s = \pm 1$ (Johnson and Lippmann[14]), and the distinct transition rates from each state to the lowest orbital $j = 0$ (for which $s = -1$) are quite different. If E_0, p, and a are used to describe the respective final-state parameters, the kinematical conditions (6) and (7) apply, and S_{fi} for photon emission is identical to that found for absorption (Sec. II of the text) up to the following modification of the photon field:

(a) for absorption: $a^\mu(x) = \dfrac{\epsilon^\mu}{(2\omega L^3)^{1/2}} e^{-ik_\nu x^\nu}$,

(b) for emission: $(a^\mu(x))^* = \dfrac{(\epsilon^\mu)^*}{(2\omega L^3)^{1/2}} e^{+ik_\nu x^\nu}$.

The differential transition rate for emission into the solid angle $d\Omega$ is given by

$$\left(\frac{dR}{d\Omega}\right)_{s=\pm 1} = \sum_{\pm} \int d\omega \frac{dn}{d\omega} \frac{1}{T} \left(\int L \frac{dp}{2\pi} \int L \frac{da}{2\pi\lambda^2} |S_{fi}|^2 \right) , \tag{A1}$$

where the summation ($\pm$) is over the photon polarizations and

$$\frac{dn}{d\omega} = \frac{L^3\omega^2}{(2\pi)^3} d\Omega$$

is the density of final states. The total transition rate (inverse of the lifetime τ) is given by integrating over $d\Omega$.

The evaluation of (A1) and the integrations over volume and photon energy (all of which involve the same δ functions encountered in Sec. II are directly analogous to the procedure used to find the absorption coefficients. The results for $s = \pm 1$ may be expressed in the integral forms

$$R_{s=1} = \frac{\alpha}{4} \int_0^\pi d\theta \sin\theta \left(\frac{E_1 - E_0}{E_0 E_1}\right) \frac{e^{-z}}{[1 - (p/E_0)\cos\theta]}$$
$$\times \left[(E_0 + m)(E_1 + m) \left(\frac{p}{E_0 + m} - \frac{q}{E_1 + m}\right)^2 (1 + \cos^2\theta) + \left(\frac{E_0 + m}{E_1 + m}\right) 2\epsilon^2 \sin^2\theta\, Z \right.$$
$$\left. - 2(E_0 + m)(2Z\epsilon^2)^{1/2} \left(\frac{p}{E_0 + m} - \frac{q}{E_1 + m}\right) \sin\theta\cos\theta \right] , \tag{A2}$$

$$R_{s=-1} = \frac{\alpha}{4} \int_0^\pi d\theta \sin\theta \left(\frac{E_1 - E_0}{E_0 E_1}\right) \frac{e^{-z}}{1 - (p/E_0)\cos\theta}$$
$$\times \left[\left(\frac{E_0 + m}{E_1 + m}\right) 2\epsilon^2 (1 + \cos^2\theta) + (E_0 + m)(E_1 + m) \left(\frac{q}{E_1 + m} + \frac{p}{E_0 + m}\right)^2 \sin^2\theta\, Z \right.$$
$$\left. - 2(E_0 + m) \left(\frac{q}{E_1 + m} + \frac{p}{E_0 + m}\right) (2Z\epsilon^2)^{1/2} \sin\theta\cos\theta \right] . \tag{A3}$$

The lifetimes for an electron initially at rest are obtained by letting $q = 0$ in each case, for which equations (A1), (A2) reduce (in conventional units) to

$$(R_0)_{s=1} \sim \frac{2}{3} \frac{\alpha}{\hbar} \left(\frac{B}{B_{cr}}\right)^3 mc^2 , \tag{A4}$$

$$(R_0)_{s=-1} \sim \frac{4}{3} \frac{\alpha}{\hbar} \left(\frac{B}{B_{cr}}\right)^2 mc^2 . \tag{A5}$$

It is thus seen that for $B \ll B_{cr}$, the emission from the state $s = -1$ proceeds much faster than that for $s = +1$ (the "spin-flip" case). However, a closer examination of the derivation of the absorption coefficients in Sec. II also reveals that the transitions to the $s = -1$ excited state are the major contributors to the absorption rate. For this reason it is the faster rate (A3) which determines the natural width Γ of the resonance in the Compton scattering cross section (see the discussion in Sec. VI).

For electrons with nonzero initial momentum q, the lifetimes may either be found explicitly by integrating equations (A2), (A3) over $d\theta$, or quite simply obtained from the well-known Lorentz transformation law $\tau = \gamma_\parallel \tau_0$, where

$$\gamma_\parallel = \frac{E_1}{m} = \frac{(q^2 + m^2 + 2\epsilon^2)^{1/2}}{m} .$$

A comparison of the two methods in fact provides a useful check on the algebraic manipulations (including phases) of the first-order derivation, most of which are identical to those encountered in the calculation of the attenuation coefficients in the text.

ACKNOWLEDGMENTS

The authors would like to thank Professor Wolf-

gang Kundt and Dr. Eckhard Krotscheck for helpful discussions. We are also deeply grateful to Professor Thomas Erber for reading and commenting on the manuscript. Finally, we wish to thank Professor Joachim Trümper and Dr. Berndt Aschenbach for valuable discussions concerning the possible application of the present results to pulsating x-ray sources.

This work was supported by the Deutsche Forschungsgemeinschaft.

---

[1]The literature on magnetic bremsstrahlung is far too extensive to be summarized here, although a thorough account which covers both the classical and quantum-mechanical regimes may be found in A. A. Sokolov and I. M. Ternov, *Synchrotron Radiation* (Pergamon, New York, 1968).

[2]J. S. Toll, Ph.D. thesis, Princeton University, 1952 (unpublished).

[3]N. P. Klepikov, Zh. Eksp. Teor. Fiz. 26, 19 (1954).

[4]T. Erber, Rev. Mod. Phys. 38, 626 (1966).

[5]H.-Y. Chiu and L. Fassio-Canuto, Phys. Rev. 185, 1614 (1969).

[6]V. Canuto and H.-Y. Chiu, Sp. Sci. Rev. 12, 735 (1971).

[7]P. A. Sturrock, Astrophys. J. 164, 529 (1971).

[8]M. A. Ruderman and P. G. Sutherland, Astrophys. J. 196, 51 (1975).

[9]Yu. N. Gnedin and R. A. Sunyaev, Astron. Astrophys. 36, 379 (1974).

[10]M. M. Basco and R. A. Sunyaev, Astron. Astrophys. 42, 311 (1975).

[11]J. Trümper *et al.*, in Eighth Texas Symposium for Relativistic Astrophysics, Boston, December 1976 (unpublished).

[12]V. Canuto and J. Ventura, Fundamentals of Cosmic Physics (to be published).

[13]A previous quantum-mechanical treatment of the absorption effect, valid in the asymptotic limit for which the photon energy greatly exceeds the Landau level spacing, has been given by P. Urban and K. Wittmann, Acta Phys. Austriaca 35, 9 (1972). These authors do not consider the photon attenuation coefficients due to a continuous distribution of electron momenta.

[14]M. H. Johnson and B. A. Lippmann, Phys. Rev. 76, 828 (1949).

[15]J. D. Bjorken and S. D. Drell, *Relativistic Quantum Mechanics* (McGraw-Hill, New York, 1964).

[16]G. Szegö, *Orthogonal Polynomials*, American Math. Soc. Colloquium Publications 23 (1939).

[17]M. Abramowitz and I. A. Stegun, *Handbook of Mathematical Functions* (Dover, New York, 1965).

[18]J. J. Sakurai, *Advanced Quantum Mechanics* (Addison-Wesley, Reading, Mass., 1967).

[19]V. Canuto, J. Lodenquai, and M. Ruderman, Phys. Rev. D 3, 2303 (1971).

[20]J. Herrmann and V. Ch. Zhukovskii, Ann. Phys. (Leipzig) 27, 349 (1971).

[21]K. A. Milton *et al.*, Phys. Rev. D 10, 1299 (1974).

[22]S. S. Holt, E. A. Boldt, R. E. Rothschild, and P. J. Serlemitsos, Astrophys. J. 190, L109 (1974).

[23]S. H. Pravdo, Ph.D. thesis, University of Maryland, 1976, NASA/GSFC Report No. X-661-76-280 (unpublished).

[24]E. A. Boldt, S. S. Holt, R. E. Rothschild, and P. J. Serlemitsos, Astron. Astrophys. 50, 161 (1976).

[25]V. L. Ginzburg and S. I. Syrovatskii, Annu. Rev. Astron. Astrophys. 7, 375 (1969).

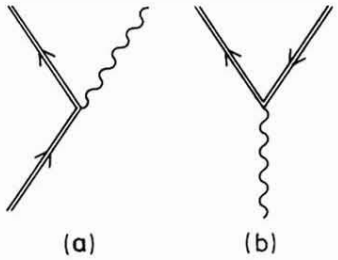

FIG. 1. First-order processes involving a single particle (electron or photon) in the initial state. The double line for the electron current denotes that the particle moves through a uniform magnetic field, so that its wave function satisfies the corresponding bound-state Dirac equation. Diagram (a) represents magnetic bremsstrahlung or synchrotron radiation, for which the emitting particle may be either a positive or negative electron. Diagram (b) denotes magnetic pair conversion of a single photon.

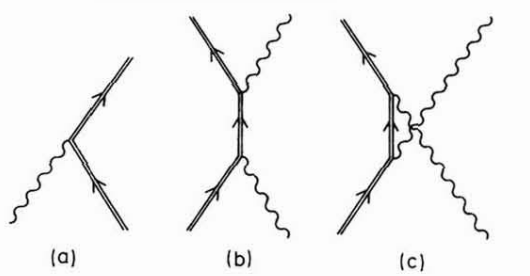

FIG. 2. (a) First-order absorption diagram. (b), (c) Compton scattering diagrams. When the kinematical conditions (6) and (7) in the text are satisfied, diagram (b) becomes equivalent to the sequential pair of diagrams 2(a) and 1(a), for which the virtual state approaches the mass shell of a real electron. Diagram (b) is responsible for the absorption resonance shown in Fig. 8 (see also Sec. VI).

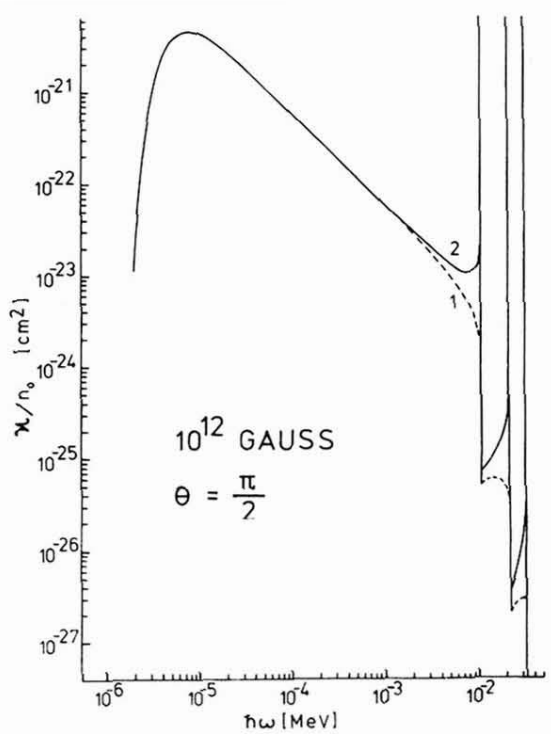

FIG. 3. Specific attenuation coefficients κ/n_0 vs photon energy for $\theta = \pi/2$, corresponding to the half-Gaussian electron momentum distribution given by Eq. (31), with $p_c = 1$ GeV. The field strength is here chosen to be 10^{12} G. The curves shown are for the two linear polarizations specified by Eq. (3). The high-energy portion of the graph displays the lowest critical frequencies at which singularities occur for both polarizations, while the smooth rollover at low energies reflects the drop in the electron spectrum above 1 GeV. The broad portion over which it is almost inversely proportional to ω (corresponding to the flat part of the electron spectrum) satisfies the approximations (28a) and (30a).

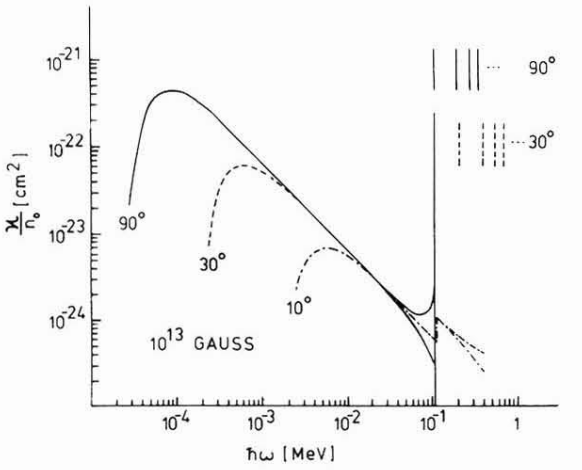

FIG. 4. The behavior of κ/n_0 vs ω at different angles of incidence for a fixed field strength, here chosen to be 10^{13} G. The assumed electron distribution is identical to that for Fig. 3. For 90° and 30° only the low-energy portions of the curves are shown (below the first critical frequency for 90°), although the upper right-hand corner indicates the shift of all the singularities toward higher frequencies as θ is decreased [see Eq. (24)]. The critical frequencies for 10° are not shown. However, the latter curve is extended above 0.1 MeV to include an abrupt increase by a factor of 2, which occurs when both the momentum solutions (26) become positive and contribute to the absorption [See Eq. (30a)].

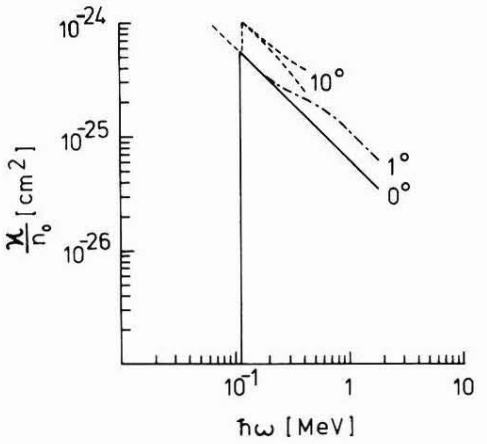

FIG. 5. Continuation of Fig. 4 to smaller angles. The factor-of-2 increase in κ/n_0 for 10° is also shown here. This may be compared with the gradual increase for 1° incidence, the difference being that for increasing frequency, the p_+ contribution is the first to appear in the former case and p_- in the latter case. For $\theta = 0$ there is only one finite-momentum solution, which is increasing with photon energy.

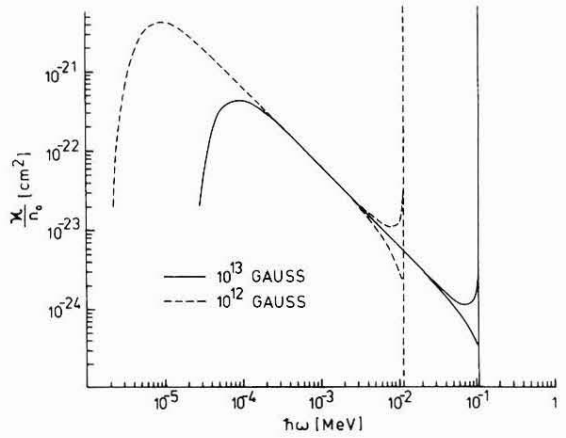

FIG. 6. Behavior of κ/n_0 for different field strengths, at fixed angle of incidence (here 90°). See discussion in Sec. V.

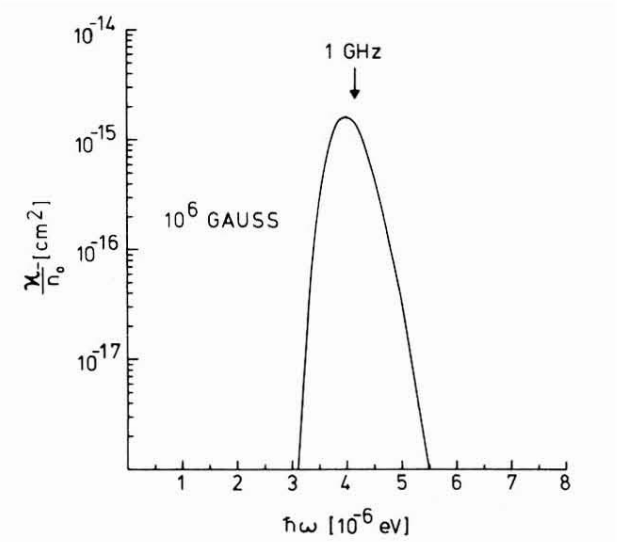

FIG. 7. Absorption at radio frequencies by a relativistic bunch of electrons in a megagauss field. A "typical" incident angle of 10° is assumed for definiteness. The postulated electron distribution has a full Gaussian shape [see Eq. (32)], with $p_0 = 9.7$ GeV and $p_c = 1.0$ GeV, these values being chosen to result in absorption at 1 GHz.

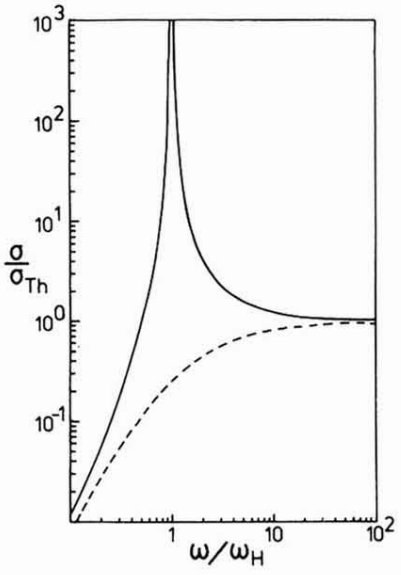

FIG. 8. Behavior of Thomson scattering cross sections for the case of parallel propagation. The solid (dashed) line refers to photons of photons of positive (negative) helicity. The absorptive resonance for positive-helicity photons, whose peak is dependent on field strength (see Appendix), occurs at the cyclotron frequency $\omega_H = (B/B_\alpha)\, mc^2$ for electrons at rest.